Journal of Molecular Modeling (2018) 24: 277
https://doi.org/10.1007/s00894-018-3813-6

ORIGINAL PAPER

Influence of dislocations, twins, and stacking faults on the fracture behavior of nanocrystalline Ni nanowire under constant bending load: a molecular dynamics study

K. Vijay Reddy[1] · Snehanshu Pal[1]

Received: 15 May 2018 / Accepted: 27 August 2018 / Published online: 8 September 2018

Abstract

In this paper, constant load bending tests were performed on a nanocrystalline Ni nanowire specimen at different deformation temperatures using molecular dynamics simulation to investigate deformation behavior and mechanisms responsible for fracture. The nature of the fracture occurred in this nanowire specimen is found to transit from brittle to ductile as the temperature rises from 500 to 800 K. Also, with an increase in temperature, the fracture strain is increased indicating more plastic deformation prior to fracture. In the case of 500 K and 600 K deformation temperatures, fracture occurred along the shear band due to slip-twin interaction. On the other hand, at comparatively higher deformation temperatures, such as 700 K and 800 K, twinning and detwinning mechanisms are responsible for accommodating large plastic strain before fracture thus imparting plasticity in the specimen. It has also been found that formation and collapse of the stacking fault tetrahedron causes fracture of nanocrystalline Ni nanowire at 800 K.

Keywords Ni nanowire · Bending test · Plasticity · Molecular dynamics

Introduction

Metallic nanowires (NWs) have gained enormous attention in recent years because of their superior mechanical properties [1–5]. In particular, metallic nanowires possess very high yield and fracture strength, and because of these favorable properties, they are widely used in nanoelectronics and nanoelectromechanical (NEMS) applications [6–8]. In quest of understanding the underlying mechanism behind such superior properties and mechanical performances, researchers have recently conducted intensive studies on metallic nanowires. For instance, Lu et al. [9] and Chen et al. [10] predicted that the surface nucleated dislocations controls the deformation process thus mediating ultra-high strength in the nanowire specimens. In another study, Wang et al. proposed that the presence of angstrom-level twins in the Au nanowires can enhance the tensile strength up to theoretical values [11]. They found that the presence of twins leads to homogeneity in the dislocation nucleation as well as shear localization. Zhu et al. [12] experimentally studied the tensile properties of fivefold twinned Ag nanowires and observed that elasticity, yielding, and the fracture is highly dependent on the size of the nanowire specimen. Apart from experimental studies, various simulation techniques, such as ab initio calculations [13], finite element method (FEM) [14], and molecular dynamics (MD) simulations [15, 16] have also been used to study the properties and performance of metallic nanowires. In most studies present in the literature, tensile and compressive tests have been performed to investigate the mechanical properties of the metallic nanowires. However, from the application perspective, these nanowires are typically used in stretchable and flexible electronics that undergo extensive bending loads [17–19]. Hence, bending test studies become important in characterizing the deformation behavior of metallic nanowires. Moreover, bending tests are preferred over tensile tests because deformation analysis using tensile tests is difficult due to imperfect gripping of specimens [20]. Some scattered literature studies are available investigating the bending deformation behavior of nanowires at an atomistic level [20–22]. For

Electronic supplementary material The online version of this article (https://doi.org/10.1007/s00894-018-3813-6) contains supplementary material, which is available to authorized users.

✉ Snehanshu Pal
pals@nitrkl.ac.in

[1] Department of Metallurgical and Materials Engineering, National Institute of Technology Rourkela, Rourkela 769008, India

instance, Deb Nath [20] studied the elastic and elastic-plastic properties of face centered cubic (FCC) specimens through bending deformation tests using molecular dynamics simulation, whereas Zhan et al. [21] studied the effect of position of preexisting defect on the bending properties of the Ag nanowire specimen. These molecular dynamics based simulation studies on nanowire bending deformation have been conducted at a constant strain rate, i.e., variable load with respect to time. However, for sufficiently thin metallic nanowires, constant applied load bending deformation analysis is another important area of research to study the mechanical properties [23]. Due to high surface area and grain boundary (GB) diffusion, constant loading tests shows a "Coble creep" like plastic deformation in such materials. Despite the vast scope of atomistic modeling in studying the constant applied load deformation behavior at nanoscale [24–26], only one molecular dynamics simulation based study of constant load bending deformation is available in the literature [27]. In actual fact, the deformation mechanism of nanocrystalline material during constant applied bending load is elusive till date and a comprehensive exploration is essential. In this present molecular dynamics study, the constant load bending test of nanocrystalline (NC) Ni nanowire specimen was performed. This paper mainly focuses on the underlying mechanism of deformation and fracture behavior of the NC Ni nanowire specimen for various temperatures. The effect of twins and twin boundary, stacking fault, and twin-slip interactions has also been investigated and reported in detail herein.

Computational methods

A nanocrystalline (NC) Ni nanowire specimen with a cross-sectional dimension of (14×14) nm and a length of 70 nm is considered for this study. The initial specimen was generated using the open source tool Atomsk [28]. The tool generates the NC specimen based on an algorithm which first creates uniformly distributed nodes in the three dimensional simulation box as shown in Fig. 1a. These nodes are then linked to each other by straight lines (illustrated as red lines in Fig. 1b). The aforementioned process is followed by another algorithm that generates the grain contours normal to the red lines (represented by blue lines in Fig. 1c). After the formation of grain contour, atomic unit cells with different orientations are expanded, which finally leads to formation of the NC specimen as shown in Fig. 1d. The average grain size of the NC specimen is approximately 6 nm and the total number of atoms present is 1,264,646 atoms. For performing the deformation tests, both ends of the specimen are fixed and a constant bending load of 8 pN is applied along the positive Z-direction, i.e., [0 0 1] direction as shown in Fig. 2. The bending deformation process was carried out at various temperatures, i.e., 500 K, 600 K, 700 K, and 800 K. The molecular dynamics simulations were performed using Large-scale Atomic/Molecular Massively Parallel Simulator (LAMMPS) software [29]. The inter-atomic interactions were described using embedded atom method (EAM) potential for Ni developed by Mendelev et al. [30]. Nonperiodic with shrink wrapped boundary conditions are used along X-, Y-, and Z- directions. Before applying the constant bending load, the energy minimization process for the specimen was carried out using the conjugate gradient method [29]. After minimization, the specimen is equilibrated for each deformation temperature under canonical (NVT) ensemble by employing Nosé-Hoover thermostat [31]. A time step of 0.002 ps is considered for this molecular dynamics simulation study. OVITO [32] software was used to visualize and analyze the atomic configurations during the bending deformation process of NC Ni nanowire. Common neighbor analysis (CNA) [33], dislocation analysis (DXA) [34], and atomic strain analysis [35, 36] were performed during the deformation process of the specimen. CNA helps in the determination of the local crystalline structure of atoms in the specimen by decomposing the radial distribution function (RDF). Mathematically, radial distribution function (RDF) is expressed through the following equation [37]:

$$g(r) = \frac{V}{N^2}\left(\sum_{i=1}^{N}\frac{n(r)}{4\pi r^2 \Delta r}\right) \quad (1)$$

where V is total volume, N is the total number of atoms, and $n(r)$ is the available number of atoms between distance of r

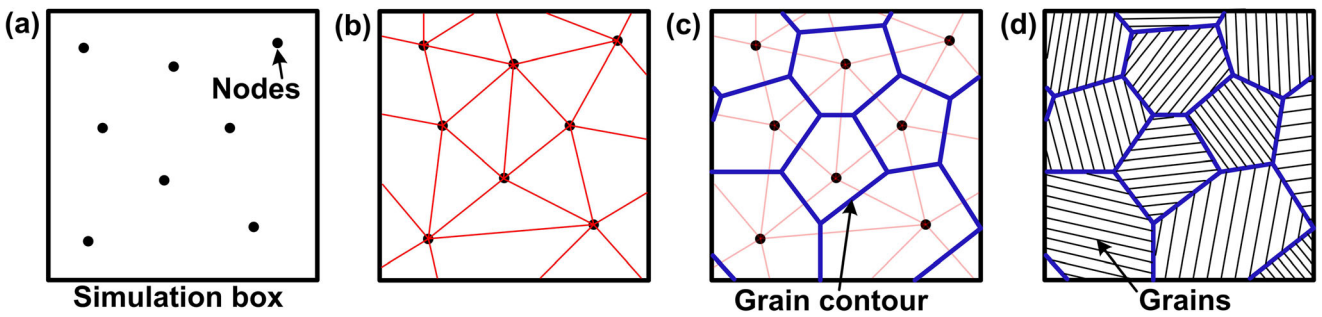

Fig. 1 Schematic illustration of the generation of nanocrystalline Ni specimen

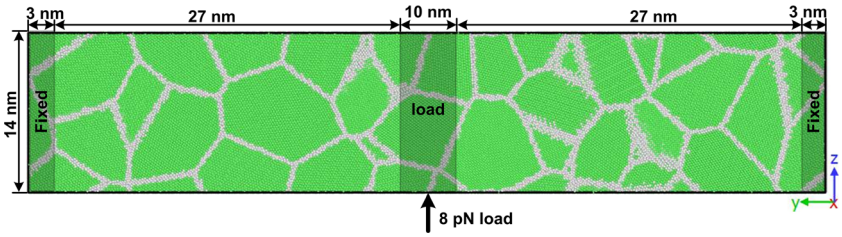

Fig. 2 A common neighbor analysis (CNA) illustration of nanocrystalline Ni nanowire specimen subjected to a bending load of 8 pN. Shaded regions in the specimen specify fixed and loading sections

and $(\boldsymbol{r} + \Delta \boldsymbol{r})$. The decomposed RDF relation through which CNA is expressed is given by the following equation [38]:

$$g(r) = \sum_{jkl} g_{jkl}(r) \tag{2}$$

CNA analysis assigns three indices, i.e., *j, k, l*, to every pair of atoms in a specimen and the assigned set of indices signifies the local environment of the pair. The first index, *j*, signifies the number of neighbors common to the two given atoms. The second index, *k*, denotes the the number of bonds among those neighbors. The third index, *l*, is the number of bonds in the longest continuous chain formed by the *k* bonds among the common neighbors. These computed indices (*j, k, l*) values are then compared with a set of reference signatures to determine the local crystal structure of the specimen. On one hand, identification of various partial and perfect dislocations generated during the bending process was done by performing the DXA, whereas the generation of tensile, compressive, and shear strain in the specimen was investigated using atomic strain analysis.

To calculate the bending strain, first deflection of the nanowire was identified and accordingly the change in length of the central plane (ΔL) was calculated using the following mathematical relation [39]:

$$\Delta \boldsymbol{L} = \frac{\mathbf{12}}{\mathbf{5}} \frac{\boldsymbol{\delta}^{\mathbf{2}}}{\boldsymbol{L}} \tag{3}$$

where δ is deflection in the nanowire and L is the total length.After finding out the change in length of the central plane (ΔL), the strain was calculated using the following mathematical relation:

$$\varepsilon = \frac{\Delta \boldsymbol{L}}{\boldsymbol{L}} = \frac{\mathbf{12}}{\mathbf{5}} \frac{\boldsymbol{\delta}^{\mathbf{2}}}{\boldsymbol{L}^{\mathbf{2}}} \tag{4}$$

where ε is strain during the bending deformation process of NC Ni nanowire specimen.

Results and discussion

Analysis of variation in bending strain and dislocation densities during simulated bending test

The bending deformation behavior of the NC Ni nanowire specimen at constant applied load and different temperatures is reported herein. Figure 3a presents the bending strain vs. time curve for the specimen deformed at 500 K (black line), 600 K (red line), 700 K (blue line), and 800 K (green line). It is observed that with an increase in the time period, the strain rate increases for all temperatures. From Fig. 3a, it is also observed that the NC Ni nanowire specimen is found to be fractured at 460 ps, 470 ps, 458 ps, and 440 ps during the bending deformation at 500 K, 600 K, 700 K, and 800 K respectively. This indicates that the increase in temperature causes a rapid failure of the specimen with an exception of deformation at 500 K where an early fracture occurs (For a detailed discussion, refer to section "Bending deformation

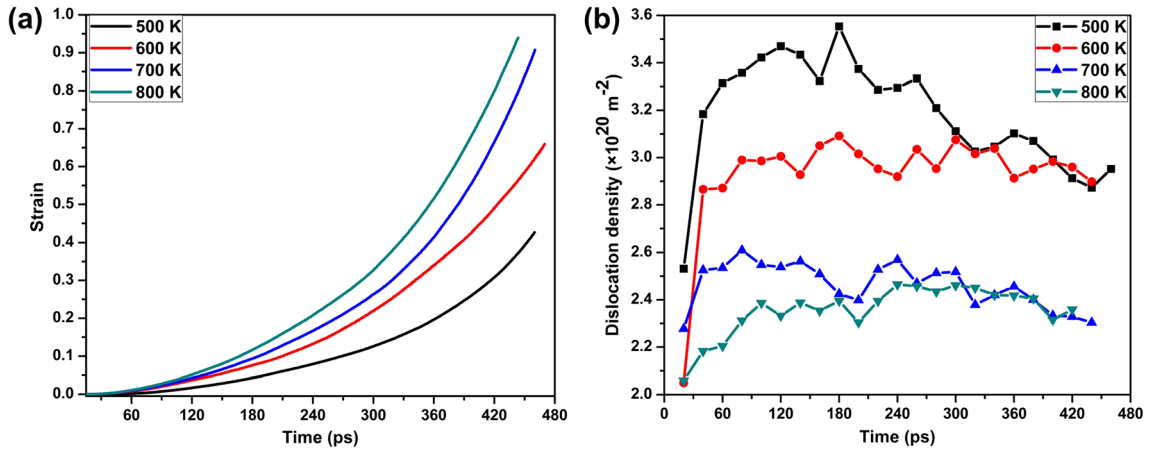

Fig. 3 **a** Plots between strain and time during the constant load bending deformation of nanocrystalline Ni nanowire specimen at various temperatures. **b** Variation in dislocation density with respect to time during the deformation of the specimen

behavior at 500 K"). Also with an increase in temperature, the strain rate has increased indicating a higher plastic deformation due to grain movement and lattice diffusion process, which is at par with the findings substantiated in previous literature [40, 41]. Figure 3b shows the plot for variation in the dislocation density during bending of the NC Ni nanowire at different temperatures. A common trend is observed in the plot in which the dislocation density first increases rapidly and then attains a steady state followed by a decrease at the end of the deformation. A higher dislocation density is observed for the specimen deformed at 500 K, which indicates that dislocation mediated deformation is the prevailing mechanism [42]. As the temperature is increased, it is observed that the dislocation density decreases indicating that the diffusion mediated deformation process becomes more active at higher temperatures. Figure 4 shows the plot of variation in volume fraction of atoms under compressive strain vs. temperature at different time periods. It is observed that with the increase in the temperature, the volume fraction of atoms with compressive strain decreases. Representative snapshots (shown as inset in Fig. 4) at an initial time period of 60 ps show that at 500 K, compressive strain is distributed at grain boundaries as well as grain interior. It is evident from the inset picture (of Fig. 4) that the compressive strain present in the grain interior decreases as the temperature increases, and the compressive strain is mostly distributed at the grain boundary. Also with the increase in time period, the compressive strain in the specimen is reduced, while tensile and shear strain is increased in the specimen. Figure 5 shows the plot of variation in fracture strain and time of fracture with respect to deformation temperature for the NC Ni nanowire specimen. The maximum strain attained before failure is found to be 42.6%, 65.9%, 90.7%, and 93.9% in case of deformation at 500 K, 600 K, 700 K, and 800 K respectively. On the other hand, it is observed that the fracture time is 460 ps, 470 ps, 458 ps, and 440 ps during the bending deformation at 500 K, 600 K, 700 K and 800 K respectively. From Fig. 5, it is inferred that the failure of specimen deformed at 500 K is caused by brittle fracture as the fracture strain as well as fracture time is low, whereas the NC Ni nanowire at 800 K undergoes plastic deformation before the occurrence of fracture as the fracture strain is highest. A detailed discussion is presented in the subsequent sections that explains the underlying mechanism of fracture at various deformation temperatures.

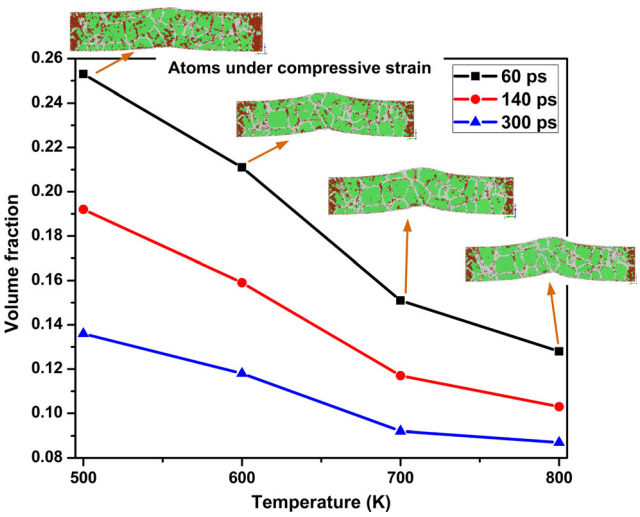

Fig. 4 Plots of volume fraction of atoms under compressive strain vs. deformation temperature at different time periods. (inset) CNA snapshot of the specimen showing the atoms under compressive load (brown color) at 60 ps

Bending deformation behavior at 500 K

Figure 6 illustrates the atomic strain snapshots of the cross-sectioned NC Ni nanowire specimen during the bending deformation at 500 K. It is observed that the bending deformation occurred through slip and twinning mechanism, and the failure of the specimen occurred by means of cleavage fracture. At an initial time period of 60 ps, Fig. 6a shows that a small magnitude of shear strain is generated along the grain boundaries at the lower portion of the specimen. With the increase in time period, the shear strain in the specimen increases along the grain boundary as shown in Fig. 6b. The upper portion, which is the tensile region, experiences higher shear strain when compared to that of the lower portion of the specimen. Also, slip bands are found to be generated in the nanocrystalline specimen as shown in Fig. 6b and c. It is observed that the slip bands are formed either from the surface of the specimen or from one end of the grain boundary to the other end in the grain interior. Also from Fig. 6c, it is seen that the slip bands present in the different grains have different orientations, as slip band are formed in the same crystallographic orientation as that of the

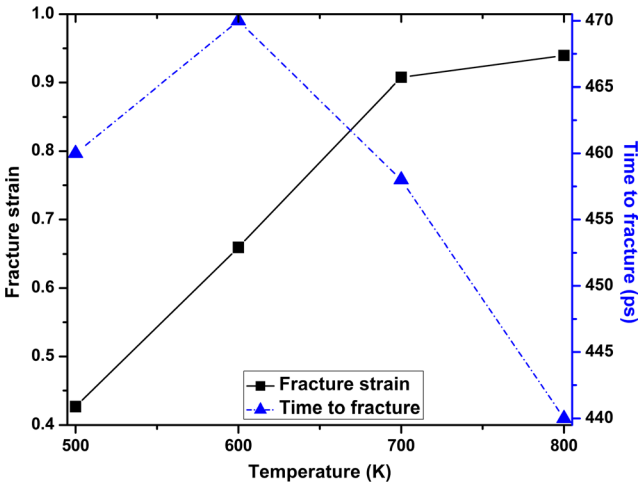

Fig. 5 Plots of variation in fracture strain and time of fracture with respect to deformation temperatures during the constant load bending deformation

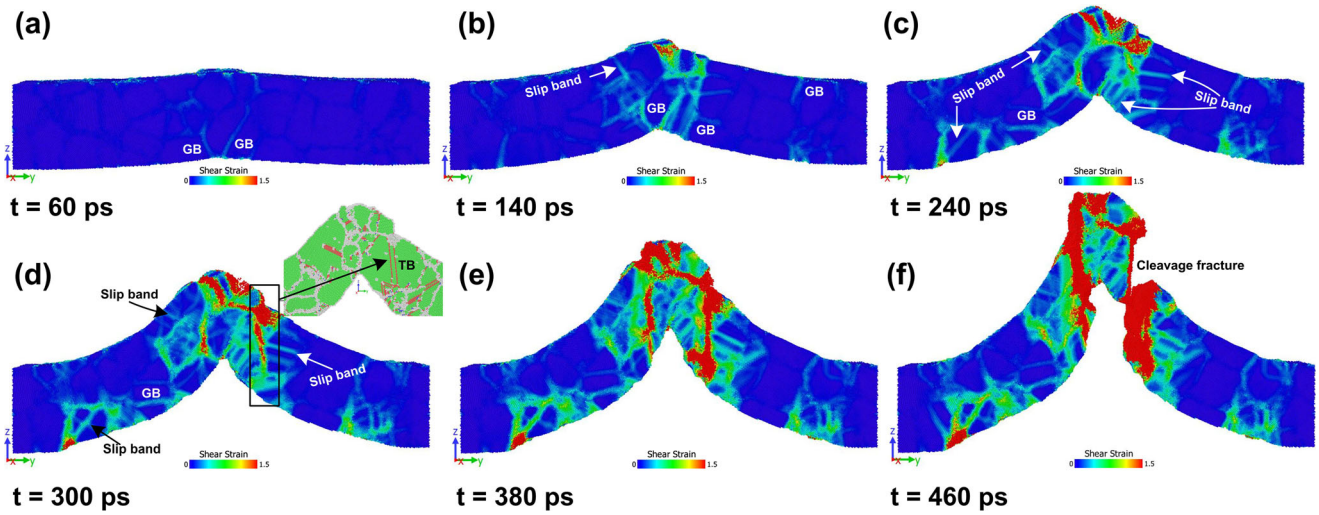

Fig. 6 Atomic strain snapshots of the nanocrystalline Ni nanowire specimen during bending deformation at 500 K at a time period of: **a** 60 ps, **b** 140 ps, **c** 240 ps, **d** 300 ps, **e** 380 ps and **f** 460 ps. (inset) CNA snapshot of the bent section at a time period of 300 ps showing the presence of twin boundaries. GB indicates grain boundaries

orientation of the corresponding grain, and this kind of phenomenon is also reported in the literature [43]. On the other hand, shear bands are formed in the noncrystallographic orientations and can traverse through interfaces from one grain to the other grain. Figure 6d and e illustrates the phenomenon of formation and propagation of shear band during the constant load bending deformation process at 500 K. Initiation of shear band formation occurs during the slip band and twin interaction as shown in Fig. 6d. The CNA snapshot (refer inset in Fig. 6d) shows the presence of twin boundaries near the bent portion of the specimen. This shear band formation is due to slip-twin interaction [44]. On further increase in time, the shear band propagates along the specimen (refer Fig. 6e), and finally the failure of the specimen occurs through cleavage fracture as shown in Fig. 6f.

The fracture mechanism during the constant load bending deformation at 500 K is shown in Fig. 7. The CNA snapshot of the cross-sectioned specimen at a time period of 400 ps is illustrated in Fig. 7a. It was previously observed that the cleavage fracture was initiated due to the shear band formation along the (2–1 0) plane. Figure 7b shows the corresponding snapshot of the various partial and perfect dislocations generated in the specimen. It is observed from the dislocation analysis that a network of 1/6 < 1 1 2 > Shockley partial screw dislocations is present at the right portion ((2–1 0) plane) of the bent specimen (refer to inset in Fig. 7b) and twin boundaries are also observed present at the exact location of the specimen. This indicates that the presence of twin boundaries is responsible for the stacking of the partial dislocations, and similar findings are also reported by other researchers [45, 46]. Also, twin boundary-slip band interactions experience significant shear strain and are known to promote crack initiation in nanocrystalline specimens due to the stacking of partial dislocations on the twin boundary plane [47]. Hence, it is indeed clear from this present study, that the specimen failed because of cleavage fracture which was initiated by the crack formation along the (2–1 0) plane during the bending deformation occurring at 500 K. A detailed demonstration of the constant load bending deformation process at 500 K is shown in movie S1.

Bending deformation behavior at 600 K

Figure 8 shows the atomic strain snapshot (shear strain) during the constant load bending deformation process at 600 K. Similar to the deformation at 500 K, the generation of shear strain occurred from the lower portion of the specimen at an initial time period of 60 ps as shown in Fig. 8a. With an increase in time period to 140 ps, the shear strain increases along the grain boundaries, and also the slip bands are formed as shown in Fig. 8b. During the deformation at 600 K, the intensity of shear strain generated in the specimen is slightly higher when compared to that of deformation at 500 K. It is observed from Fig. 8c that the initiation of shear band formation in the specimen started at a time period of 240 ps. With further increase in time, a comparatively broader shear band is propagated along the right portion of the specimen as shown in Fig. 8d and e. This is attributed to the fact that the width of the shear band due to strain localization is considerably dependent on the deformation temperature and this phenomenon was already observed in deformation of metallic glasses [48]. Figure 8f shows the complete fracture of the NC Ni nanowire specimen, which occurred at a time period of 470 ps. It is observed that the specimen fractured by means of two modes of failure, i.e., cleavage fracture at the bottom portion of the specimen and ductile fracture at the top portion of the

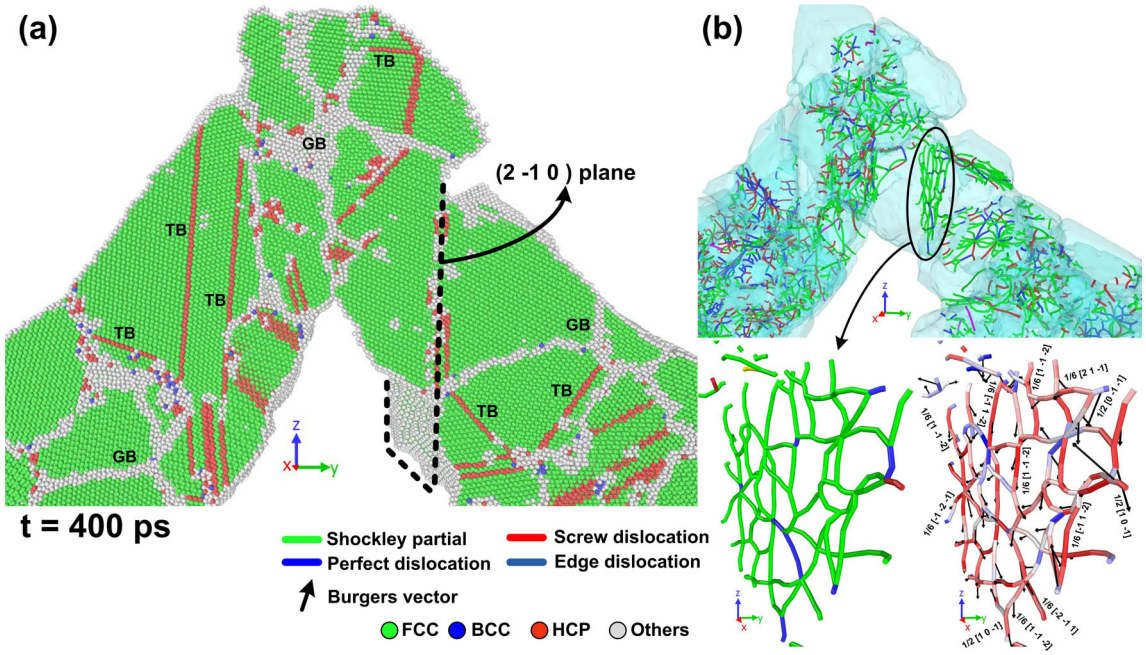

Fig. 7 **a** CNA snapshot of the bent section of the specimen deformed at 500 K, **b** Corresponding snapshot illustrating the distribution of perfect and partial dislocations. (inset) Magnified view of the network of Shockley partial dislocations present in the right portion of the bent section of the specimen. GB indicates grain boundaries, TB indicates twin boundaries

specimen. The fracture mechanism during the bending deformation process at 600 K is illustrated in Fig. 9. Figure 9a shows the CNA snapshot of the bent specimen at a time period of 360 ps, and it is observed that the cleavage fracture initiates from the bottom portion of the specimen along the (2–1 0) plane. Correspondingly, Fig. 9b shows the perfect and partial dislocations generated at the exact location in the bent section of the specimen. Similar to deformation at 500 K, a network of 1/6 < 1 1 2 > Shockley partial screw and mixed dislocations is observed in the specimen (refer to inset of Fig. 9b). However, in the case of deformation at 600 K, the network of dislocations is present only at the bottom portion of the specimen, whereas very few dislocations are present at the top portion of the specimen. This indicates the presence of twin boundary at the bottom portion of the specimen, which caused the stacking of the partial dislocations and aided in the cleavage fracture. On the other hand, the presence of grain boundary along the top portion of the (2–1 0) plane acts as resistance to the

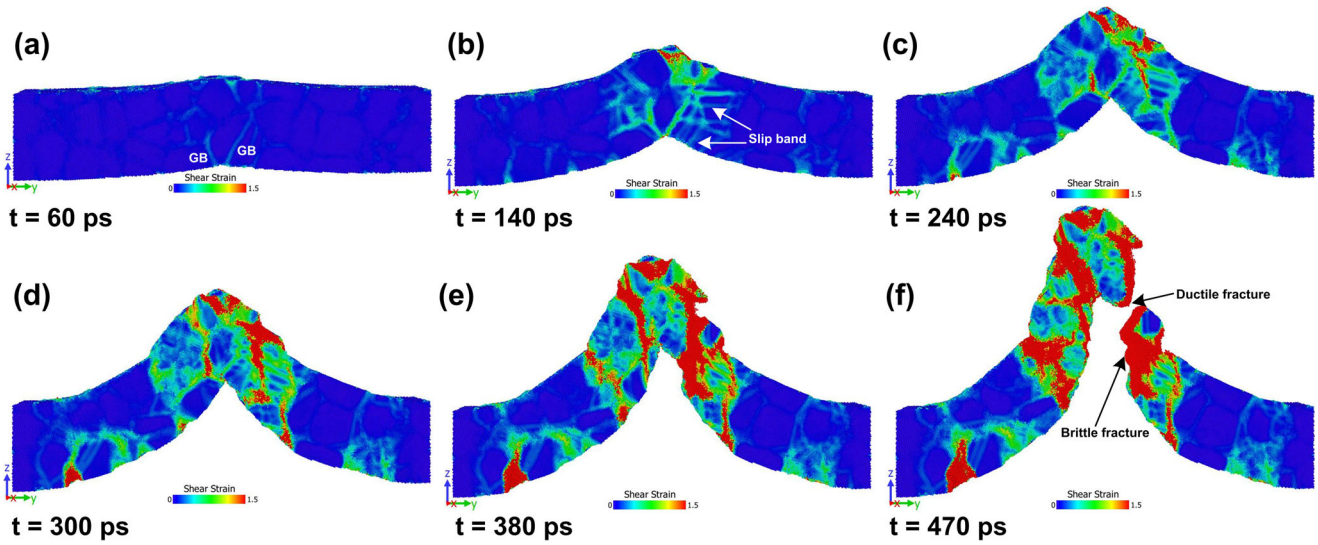

Fig. 8 Atomic strain snapshots of the nanocrystalline Ni nanowire specimen during bending deformation at 600 K at a time period of: **a** 60 ps, **b** 140 ps, **c** 240 ps, **d** 300 ps, **e** 380 ps, and **f** 470 ps. GB indicates grain boundaries

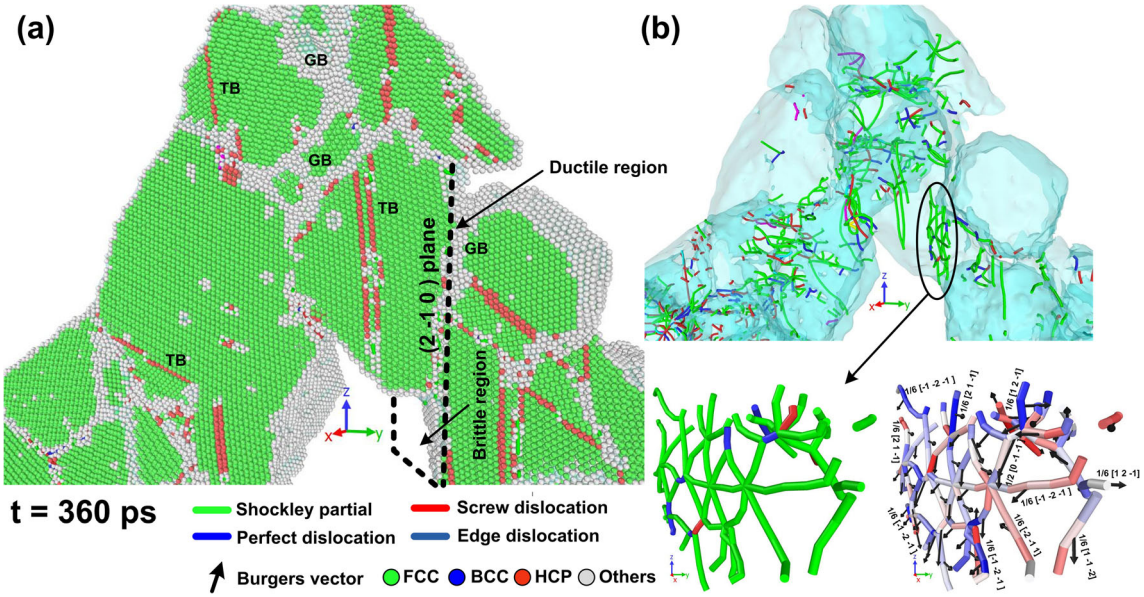

Fig. 9 **a** Illustration of CNA snapshot of the bent section of the specimen deformed at 600 K, **b** Corresponding snapshot showing the distribution of perfect and partial dislocations. (inset) Magnified view of the network of Shockley partial dislocations present in the right portion of the bent section of the specimen

shearing of the specimen. A recent literature study also reported that the presence of high misorientation grain boundary helps in arresting the shearing or cracking of specimen [49]. The presence of grain boundary at the top portion causes the ductile fracture through necking. The cleavage fracture along the twin boundary at the bottom portion and ductile fracture at the top portion of the specimen is demonstrated in movie S2.

Bending deformation behavior at 700 K

Figure 10 shows the atomic strain snapshots during the constant load bending deformation behavior of the NC Ni nanowire specimen at 700 K. Because of comparatively higher deformation temperature, intensive shear strain is generated along the grain boundaries at the lower portion of the specimen as shown in Fig. 10a. With an increase in time, a rapid increase in the shear strain is observed as shown in Fig. 10b and c. Though the shear bands are formed in the specimen at a time period of 320 ps (refer to Fig. 10d), the complete fracture of the specimen did not occur until 458 ps indicating occurrence of plastic deformation. Figure 10e shows the formation of extensive plastic zone at the right portion of the specimen followed by necking initiation, and finally, the failure of the specimen occurred through ductile fracture as shown in Fig. 10f. It was identified that the formation of extensive plastic zone during deformation at 700 K is due to the twinning and detwinning mechanism. Figure 11 illustrates the deformation mechanism during the bending process at 700 K with an emphasis on twinning, dislocation-twin interaction, and detwinning process. Figure 11a shows a two dimensional representation of Thompson tetrahedron on the twin boundary of the specimen. In general, the Thompson tetrahedron helps in describing the types of dislocations which might be reacting with the twin boundaries [50, 51]. In this present study, the twin boundary-dislocation interaction obtained from the CNA and dislocation analysis was correlated with the Thompson tetrahedron to validate the detwinning process. On the other hand, Fig. 11b shows CNA snapshot of the twinned specimen at a time period of 400 ps. The inset shows only the hexagonal closed packed (HCP) atoms along with the dislocations by shrinking the atomic size of other atom types present in the specimen. It was observed that up till 400 ps, a considerable elongation occurred in the right portion of the specimen and the shear strain is accommodated by the increase in the spacing of twin boundaries. This phenomenon of increase in the spacing of twin boundaries is known to increase the plasticity of the nanocrystalline specimen [11]. However, at 400 ps, detwinning and necking processes start to occur simultaneously in the specimen (refer to Fig. 10e). The detwinning mechanism is known to induce softening and partly increase the plasticity [52], whereas the necking process causes instability in the specimen leading to fracture. The detwinning mechanism occurring in the right portion of the deformed specimen is illustrated in Fig. 11c. It is observed from dislocation analysis that the 30° Shockley partial dislocation (30° indicates angle between dislocation and burger vector) interacts with the twin boundary leaving behind a trail of stacking fault as shown in Fig. 11c. As per the Thompson tetrahedron (refer to Fig. 11a), this partial dislocation **Bγ**, having burgers vector 1/6 [−1–2 1], slips

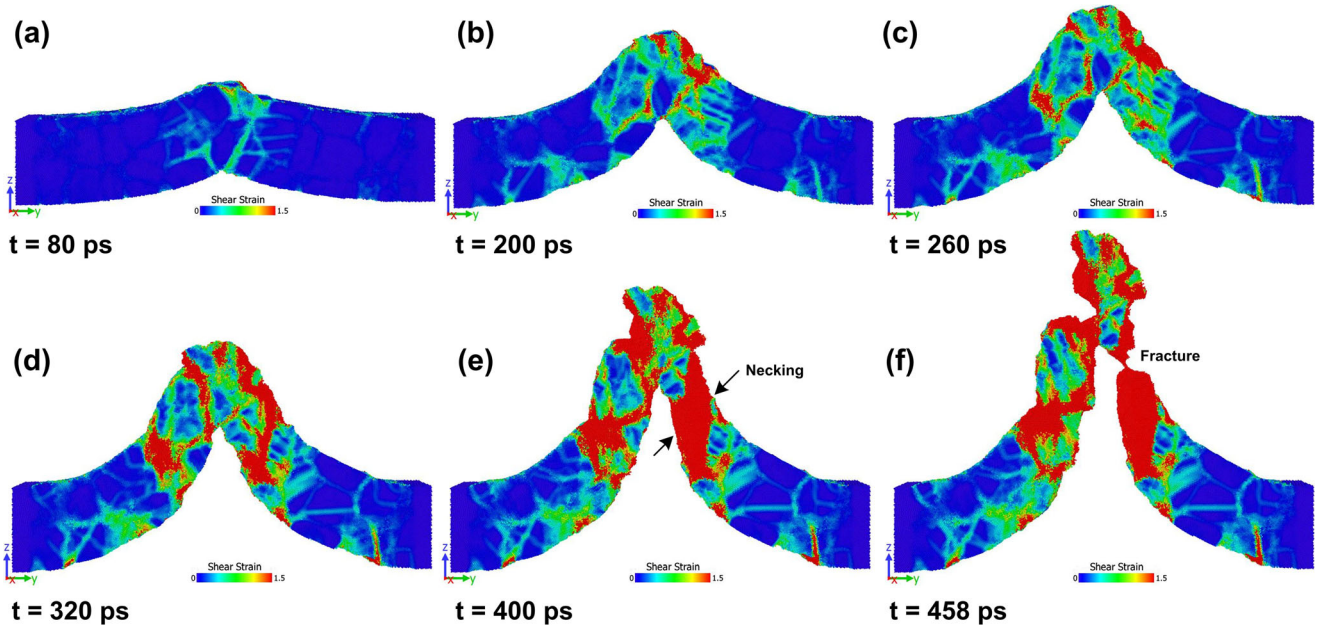

Fig. 10 Atomic strain snapshots of the nanocrystalline Ni nanowire specimen during bending deformation at 700 K at a time period of: **a** 80 ps, **b** 200 ps, **c** 260 ps, **d** 320 ps, **e** 400 ps, and **f** 458 ps

on the BAD plane to react with the twin boundary. Under constant applied load, the dissociation of the partial dislocation occurs through the following reaction:

$$\mathbf{B}\gamma \rightarrow \mathbf{B}\delta + \delta\gamma \quad (5)$$

The partial dislocation **Bδ** has a burgers vector of 1/6 [−2–1 -1] as shown in the dislocation snapshot of Fig. 11c. It is observed that the movement of partial dislocation **Bδ** toward the left of the twin causes a step in the twin boundary and leaves a stair-rod dislocation (sessile dislocation with burgers vector 1/2 [−1 1 0]) and this is the cause for the detwinning mechanism. This mechanism of twin-dislocation interaction and the formation of sessile dislocation was theoretically studied and reported in literature [53]. The complete mechanism of twin boundaries spacing during twinning and detwinning is shown in movie S3.

Bending deformation behavior at 800 K

Figure 12 shows the atomic strain snapshots of the NC Ni nanowire specimen during the deformation at 800 K. Because of higher temperature and rapid lattice diffusion, the deformation occurs at a faster rate, and hence more intensive shear strain is generated in the specimen as shown in Fig. 12a–c. It was observed that at 320 ps, the plastic strain

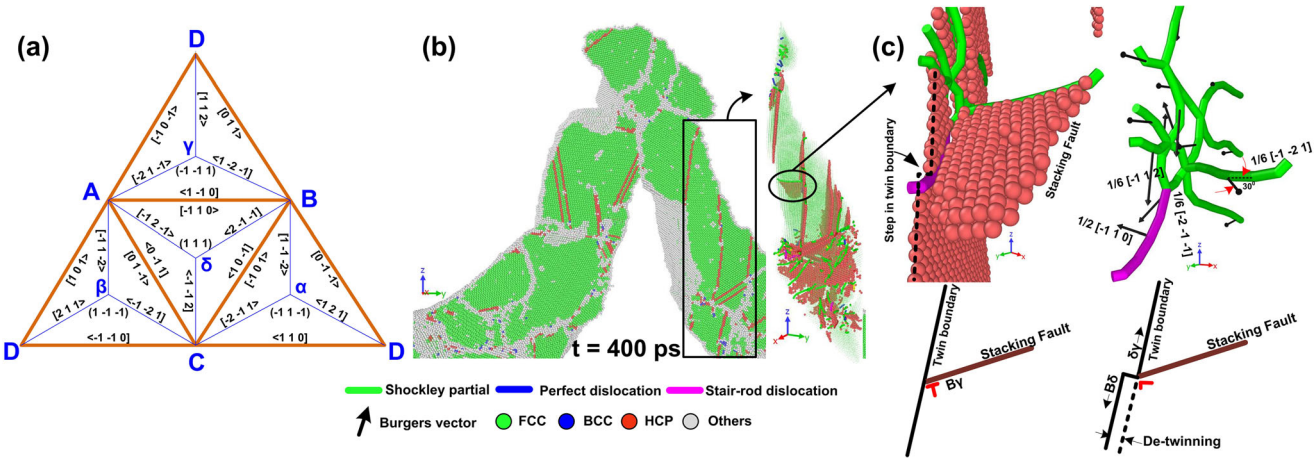

Fig. 11 **a** Schematic diagram of Thompson tetrahedron, **b** Illustration of CNA snapshot of the bent section of the specimen deformed at 700 K. (inset) illustration of HCP atoms and dislocations in the right portion of the specimen, **c** Illustration of twin-dislocation mechanism and the corresponding generation of partial dislocations

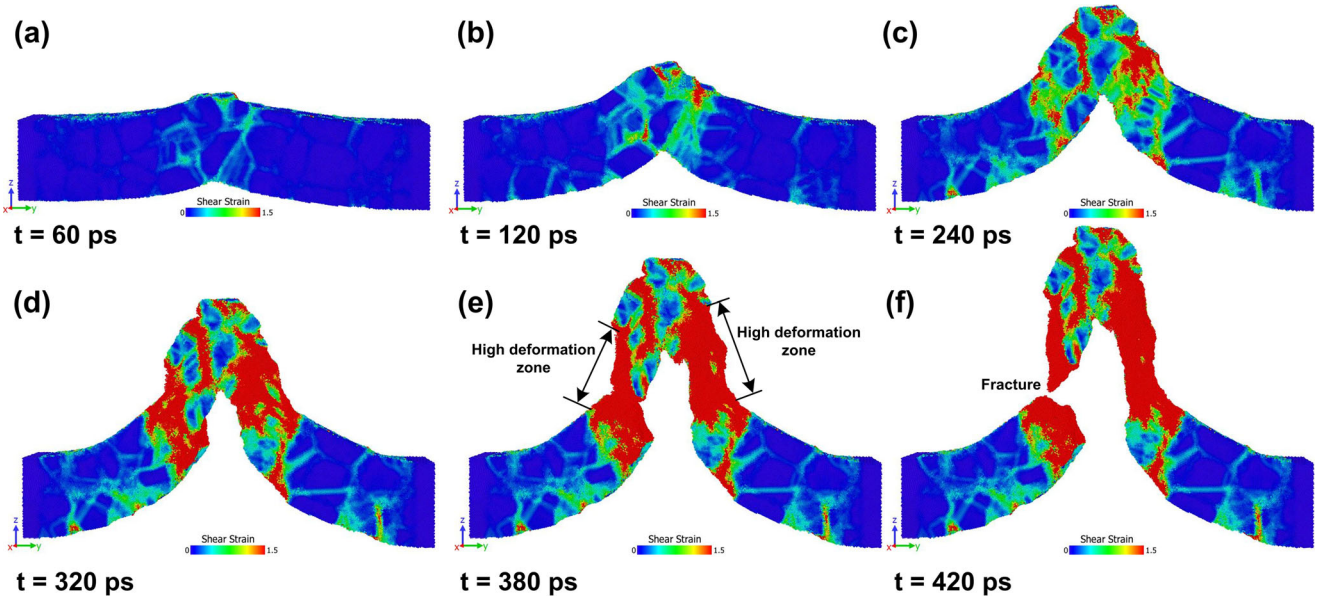

Fig. 12 Atomic strain snapshots of the nanocrystalline Ni nanowire specimen during bending deformation at 800 K at a time period of: **a** 60 ps, **b** 140 ps, **c** 240 ps, **d** 320 ps, **e** 380 ps and **f** 420 ps

was generated at both sides of the bent section as shown in Fig. 12d. With the increase in time to 380 ps (refer Fig. 12e), it was seen that further increase of plastic strain in the bent section of the specimen and necking in the left portion of the specimen occurred simultaneously. Even though the right portion of the specimen accommodates plastic strain, fracture occurred in the left portion of the specimen at 420 ps as shown in Fig. 12f. It was spotted through CNA and dislocation analysis that the cause of fracture can be due to the presence of stacking fault tetrahedrons (SFTs) in the left portion of the specimen as shown in Fig. 13. The CNA snapshot of the bent specimen along with the dislocations at 350 ps is shown in Fig. 13a. Except HCP atoms, all other atom types are shrunk to visualize the twins and stacking fault tetrahedrons. It is observed that the 1/6 < 1 1 0 > stair-rod dislocations in stacking fault tetrahedron already started to dissociate into 1/6 < 1 1 2 > Shockley partial dislocations as shown in Fig. 13b. Also, the presence of 1/3 [−1–1 -1] Frank dislocations in Fig. 13b indicates that the accumulation of vacancies helped in the formation of stacking fault tetrahedron [54]. The process of dissociation of stair-rod dislocations initially causes plasticity [55], which is also observed in the left portion of the bent section of the specimen. However, with further increase in time, this dissociation of the stair-rod dislocations leads to the collapse of the stacking fault tetrahedron present in the specimen, which causes strain localization followed by failure of the specimen [55]. Hence, we can infer that the fracture in the left portion of the specimen occurred due to the removal of

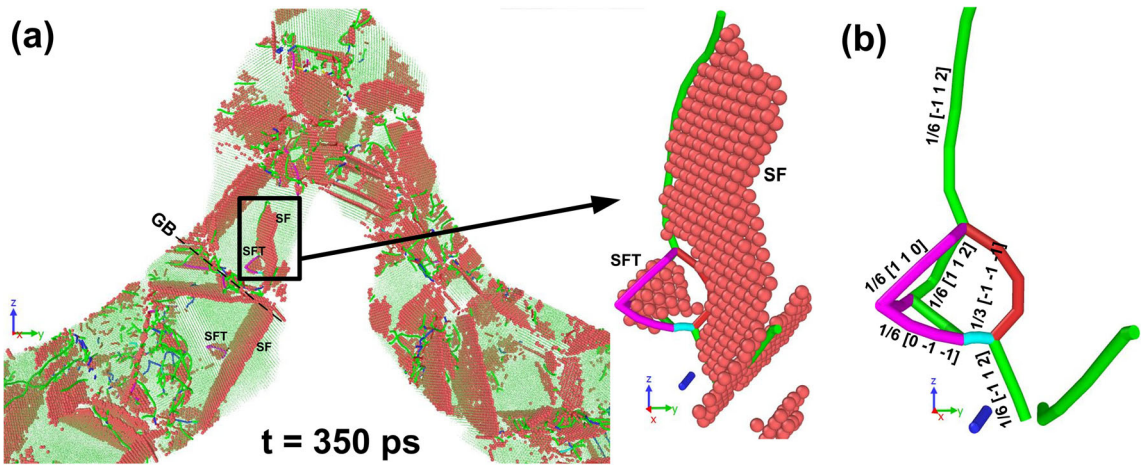

Fig. 13 **a** Illustration of CNA snapshot (showing only the magnified HCP atoms) of the bent section along with dislocations during bending deformation at 800 K. (inset) Stacking fault tetrahedron and stacking fault along with the dislocations. **b** Illustration of partial dislocations generated during the formation of stacking fault tetrahedron

SFT and the consequent strain localization process. The complete bending deformation behavior at 800 K is presented in movie S4.

Conclusions

In this paper, constant load bending deformation of the NC Ni nanowire specimen was performed at various temperatures to understand the effect of twins, slip bands, and twin-dislocation interactions. It was found that the underlying atomic scale constant load deformation mechanism is highly sensitive to temperature, as an increase in the deformation temperature transits the nature of fracture from brittle to ductile. At 500 K and 600 K, the specimen was fractured along the shear band, which is formed due to slip-twin interaction. On the other hand, at comparatively higher temperatures, ductile fracture occurred through necking of the specimen. Before fracture, large plastic strain is accommodated in the bent section of the specimen due to twinning and detwinning mechanisms. The compendium of this work can provide a rational insight to the mechanism of bending deformation of nanocrystalline materials and can contribute toward designing nanostructured materials for withstanding loads for a longer period of time without failure.

Acknowledgments The authors would like to acknowledge the Computer Centre of National Institute of Technology Rourkela for providing the high-performance computing facility (HPCF), which was essential for carrying out this molecular dynamics study.

References

1. Weinberger CR, Cai W (2012) Plasticity of metal nanowires. J Mater Chem 22(8):3277–3292
2. Wu B, Heidelberg A, Boland JJ (2005) Mechanical properties of ultrahigh-strength gold nanowires. Nat Mater 4(7):525
3. Rezaei R, Deng C (2017) Pseudoelasticity and shape memory effects in cylindrical FCC metal nanowires. Acta Mater 132:49–56
4. An BH, Jeon IT, Seo JH, Ahn JP, Kraft O, Choi IS, Kim YK (2016) Ultrahigh tensile strength nanowires with a Ni/Ni–Au multilayer nanocrystalline structure. Nano Lett 16(6):3500–3506
5. Oener SZ, van de Groep J, Macco B, Bronsveld PC, Kessels WMM, Polman A, Garnett EC (2016) Metal–insulator–semiconductor nanowire network solar cells. Nano Lett 16(6):3689–3695
6. Tian B, Zheng X, Kempa TJ, FangY YN, Yu G, Lieber CM (2007) Coaxial silicon nanowires as solar cells and nanoelectronic power sources. Nature 449(7164):885–889
7. Yu K, Major TA, Chakraborty D, Devadas MS, Sader JE, Hartland GV (2015) Compressible viscoelastic liquid effects generated by the breathing modes of isolated metal nanowires. Nano Lett 15(6):3964–3970
8. Eom K, Park HS, Yoon DS, Kwon T (2011) Nanomechanical resonators and their applications in biological/chemical detection: nanomechanics principles. Phys Rep 503(4):115–163
9. Lu Y, Song J, Huang JY, Lou J (2011) Surface dislocation nucleation mediated deformation and ultrahigh strength in sub-10-nm gold nanowires. Nano Res 4(12):1261–1267
10. Chen LY, He MR, Shin J, Richter G, Gianola DS (2015) Measuring surface dislocation nucleation in defect-scarce nanostructures. Nat Mater 14(7):707
11. Wang J, Sansoz F, Huang J, Liu Y, Sun S, Zhang Z, Mao SX (2013) Near-ideal theoretical strength in gold nanowires containing angstrom scale twins. Nat Commun 4:1742
12. Zhu Y, Qin Q, Xu F, Fan F, Ding Y, Zhang T, Wang ZL (2012) Size effects on elasticity, yielding, and fracture of silver nanowires: in situ experiments. Phys Rev B 85(4):045443
13. Elsner BAM, Müller S, Bargmann S, Weissmüller J (2017) Surface excess elasticity of gold: Ab initio coefficients and impact on the effective elastic response of nanowires. Acta Mater 124:468–477
14. Esfahani MN, Sonne MR, Hattel JH, Alaca BE (2016) Thermo-coupled surface Cauchy–Born theory: an engineering finite element approach to modeling of nanowire thermomechanical response. Mech Mater 94:46–52
15. Sepúlveda-Macías M, Amigo N, Gutiérrez G (2016) Onset of plasticity and its relation to atomic structure in CuZr metallic glass nanowire: a molecular dynamics study. J Alloys Compd 655:357–363
16. Lao J, Tam MN, Pinisetty D, Gupta N (2013) Molecular dynamics simulation of FCC metallic nanowires: a review. JOM 65(2):175–184
17. Hu L, Kim HS, Lee JY, Peumans P, Cui Y (2010) Scalable coating and properties of transparent, flexible, silver nanowire electrodes. ACS Nano 4(5):2955–2963
18. Yao S, Zhu Y (2015) Nanomaterial enabled stretchable conductors: strategies, materials and devices. Adv Mater 27(9):1480–1511
19. Lim JW, Cho DY, Eun K, Choa SH, Na SI, Kim J, Kim HK (2012) Mechanical integrity of flexible Ag nanowire network electrodes coated on colorless PI substrates for flexible organic solar cells. Sol Energy Mater Sol Cells 105:69–76
20. Nath SD (2014) Elastic, elastic–plastic properties of Ag, Cu and Ni nanowires by the bending test using molecular dynamics simulations. Comput Mater Sci 87:138–144
21. Zhan HF, Gu Y, Yan C, Yarlagadda PKDV (2014) Bending properties of Ag nanowires with pre-existing surface defects. Comput Mater Sci 81:45–51
22. Nöhring WG, Möller JJ, Xie Z, Bitzek E (2016) Wedge-shaped twins and pseudoelasticity in fcc metallic nanowires under bending. Extreme Mech Lett 8:140–150
23. Klinger L, Rabkin E (2006) Thermal stability and creep of polycrystalline nanowires. Acta Mater 54(2):305–311
24. Meraj M, Pal S (2017) Effect of temperature and stress on creep behavior of ultrafine grained nanocrystalline Ni-3 at% Zr alloy. Met Mater Int 23(2):272–282
25. Pal S, Meraj M, Deng C (2017) Effect of Zr addition on creep properties of ultra-fine grained nanocrystalline Ni studied by molecular dynamics simulations. Comput Mater Sci 126:382–392
26. Pal S, Meraj M (2016) Structural evaluation and deformation features of interface of joint between nano-crystalline Fe–Ni–Cr alloy and nano-crystalline Ni during creep process. Mater Des 108:168–182
27. Reddy KV, Meraj M, Pal S (2017) Mechanistic study of bending creep behaviour of bicrystal nanobeam. Comput Mater Sci 136:36–43
28. Hirel P (2015) Atomsk: a tool for manipulating and converting atomic data files. Comput Phys Commun 197:212–219
29. Plimpton S (1995) Fast parallel algorithms for short-range molecular dynamics. J Comput Phys 117(1):1–19
30. Mendelev MI, Kramer MJ, Hao SG, Ho KM, Wang CZ (2012) Development of interatomic potentials appropriate for simulation

of liquid and glass properties of NiZr2 alloy. Philos Mag 92(35): 4454–4469
31. Evans DJ, Holian BL (1985) The nose–hoover thermostat. J Chem Phys 83(8):4069–4074
32. Stukowski A (2009) Visualization and analysis of atomistic simulation data with OVITO–the open visualization tool. Model Simul Mater Sci Eng 18(1):015012
33. Honeycutt JD, Andersen HC (1987) Molecular dynamics study of melting and freezing of small Lennard-Jones clusters. J Phys Chem 91(19):4950–4963
34. Stukowski A, Bulatov VV, Arsenlis A (2012) Automated identification and indexing of dislocations in crystal interfaces. Model Simul Mater Sci Eng 20(8):085007
35. Shimizu F, Ogata S, Li J (2007) Theory of shear banding in metallic glasses and molecular dynamics calculations. Mater Trans 48(11): 2923–2927
36. Falk ML, Langer JS (1998) Dynamics of viscoplastic deformation in amorphous solids. Phys Rev B 57(6):7192
37. Zhang JC, Chen C, Pei QX, Wan Q, Zhang WX, Sha ZD (2015) Ab initio molecular dynamics study of the local atomic structures in monatomic metallic liquid and glass. Mater Des 77:1–5
38. Faken D, Jónsson H (1994) Systematic analysis of local atomic structure combined with 3D computer graphics. Comput Mater Sci 2(2):279–286
39. Timoshenko SP, Gere JM (1972) Mechanics of materials. Reinhold, New York
40. O'Brien CJ, Foiles SM (2016) Exploration of the mechanisms of temperature-dependent grain boundary mobility: search for the common origin of ultrafast grain boundary motion. J Mater Sci 51(14):6607–6623
41. Kim HS, Estrin Y, Bush MB (2000) Plastic deformation behaviour of fine-grained materials. Acta Mater 48(2):493–504
42. Kassner ME, Smith KK, Campbell CS (2015) Low-temperature creep in pure metals and alloys. J Mater Sci 50(20):6539–6551
43. Jia N, Eisenlohr P, Roters F, Raabe D, Zhao X (2012) Orientation dependence of shear banding in face-centered-cubic single crystals. Acta Mater 60(8):3415–3434
44. Qu S, Zhou H, Huang Z (2011) Shear band initiation induced by slip-twin boundary interactions. Scr Mater 65(8):715–718
45. Lagerlöf KPD, Castaing J, Pirouz P, Heuer AH (2002) Nucleation and growth of deformation twins: a perspective based on the double-cross-slip mechanism of deformation twinning. Philos Mag A 82(15):2841–2854
46. Chen M, Ma E, Hemker KJ, Sheng H, Wang Y, Cheng X (2003) Deformation twinning in nanocrystalline aluminum. Science 300(5623):1275–1277
47. Seita M, Hanson JP, Gradecak S, Demkowicz MJ (2015) The dual role of coherent twin boundaries in hydrogen embrittlement. Nat Commun 6:6164
48. Prasad KE, Ramamurty U (2012) Effect of temperature on the plastic zone size and the shear band density in a bulk metallic glass. Mater Sci Eng A 535:48–52
49. Pineau A, Benzerga AA, Pardoen T (2016) Failure of metals I: brittle and ductile fracture. Acta Mater 107:424–483
50. Yamakov V, Wolf D, Phillpot SR, Gleiter H (2003) Dislocation–dislocation and dislocation–twin reactions in nanocrystalline Al by molecular dynamics simulation. Acta Mater 51(14):4135–4147
51. Li PT, Yang YQ, Luo X, Jin N, Liu G, Feng ZQ (2017) Effect of rate dependence of crack propagation processes on amorphization in Al. Mater Sci Eng A 684:71–77
52. Zhu T, Gao H (2012) Plastic deformation mechanism in nanotwinned metals: an insight from molecular dynamics and mechanistic modeling. Scr Mater 66(11):843–848
53. Zhu YT, Wu XL, Liao XZ, Narayan J, Kecskes LJ, Mathaudhu SN (2011) Dislocation–twin interactions in nanocrystalline fcc metals. Acta Mater 59(2):812–821
54. Silcox J, Hirsch PB (1959) Direct observations of defects in quenched gold. Philos Mag 4(37):72–89
55. Wu L, Yu W, Hu S, Shen S (2017) Stability of stacking fault tetrahedron in twin boundary bicrystal copper under shear. Int J Plast 97: 246–258